*Electronic Supplementary Information*

# Hydrogen-evolving photocathodes consisting of $Cu_2Sn_xGe_{1-x}S_3$ particles synthesized by polymerized complex method and sulphurization

Yosuke Kageshima,*[ab] Yusuke Ooka,[a] Hiromu Kumagai,*[c] Fumiaki Takagi,[a] Katsuya Teshima,[ab] Kazunari Domen[bd] and Hiromasa Nishikiori*[ab]

[a.] Department of Materials Chemistry, Faculty of Engineering, Shinshu University, 4–17-1 Wakasato, Nagano 380–8553, Japan. E-mail: kage_ysk@shinshu-u.ac.jp; nishiki@shinshu-u.ac.jp

[b.] Research Initiative for Supra-Materials (RISM), Shinshu University, 4–17-1 Wakasato, Nagano 380–8553, Japan

[c.] Research Center for Advanced Science and Technology, The University of Tokyo, 4-6-1 Komaba, Meguro-ku, Tokyo 153-8904, Japan. E-mail: kumagai@enesys.rcast.u-tokyo.ac.jp

[d.] Office of University Professors, The University of Tokyo, 7-3-1 Hongo, Bunkyo-ku, Tokyo 113-8656, Japan

During TG-DTA analysis, the Sn EDTA complex showed significant mass loss (as high as 64%) over the temperature range of 300 to 500 °C. This was associated with an endotherm followed by an exotherm in the DTA plot (Fig. S1a). This mass loss is attributed to the simultaneous dehydration and decomposition of the organic ligands. Assuming that the monohydrated complex ($SnC_{10}H_{12}N_2O_8 \cdot H_2O$) was completely decomposed to $SnO_2$, the weight loss would be expected to be 64.5% and so it can be concluded that each complex contained a single water of hydration. In contrast, the Ge EDTA complex generated two endothermic peaks together with a mass loss of approximately 12% over the range of 100 to 300 °C. An exothermic mass loss of approximately 74% also appeared at approximately 400 °C (Fig. S1b). Assuming a dihydrate complex having the formula $GeC_{10}H_{12}N_2O_8 \cdot 2H_2O$, dehydration and complete decomposition to $GeO_2$ would be expected to provide mass losses of 10.1% and 82.0%, respectively. Therefore, it is evident that the Ge EDTA complex had two waters of hydration. These TG-DTA results are in agreement with thermal analysis data acquired under reduced pressure as previously reported in the literature.[1]

As described in the Experimental section in the main manuscript, the metal-polyamide resin was carbonized at 400 °C using a mantle heater and subsequently calcined at 550 °C in a muffle furnace to completely remove residual organic compounds. To confirm that 550 °C was sufficient to combust all organic compounds, a TG-DTA plot was obtained for a particulate specimen prepared by the PC method with subsequent carbonization at 400 °C and the results are presented in Fig. S2. These data indicate that the mass loss of this specimen essentially plateaued at 550 °C. Because this mass loss represents the evaporation of residual carbon compounds, it is apparent that only the corresponding oxide remained. Hence, it was concluded that calcination at 550 °C removed all residual organic substances.

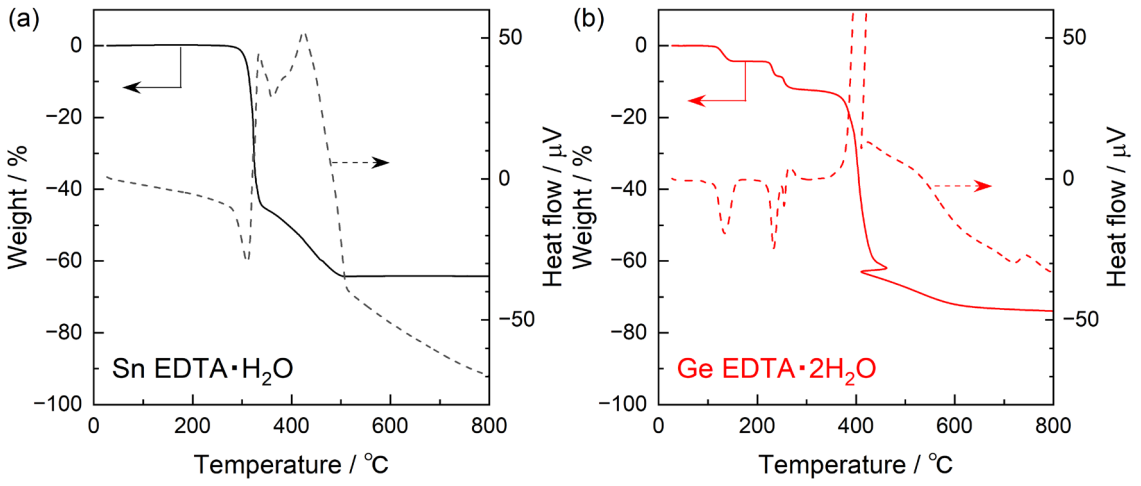


**Fig. S1** TG-DTA curves obtained from the (a) Sn EDTA·$H_2O$ and (b) Ge EDTA·$2H_2O$ complexes.

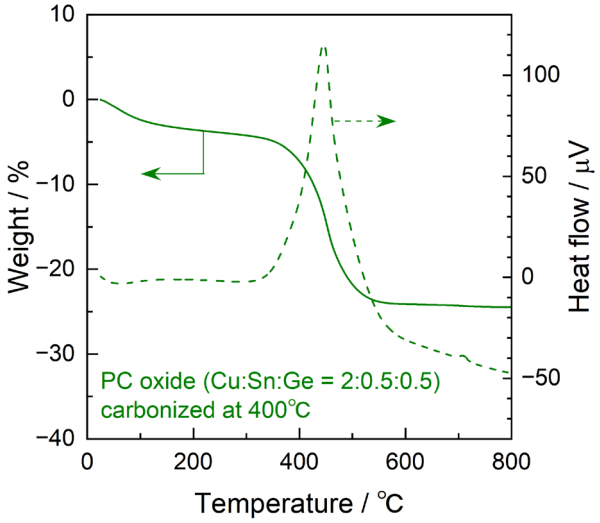


**Fig. S2** TG-DTA curve obtained from oxide particles ($x$ = 0.5) generated by the PC method and carbonized at 400 °C in a mantle heater.

The oxide precursor prepared by the PC method was heated under a continuous flow of $H_2S$ in a tubular furnace to obtain CTGS particles and the sulphurization temperature was optimized, as shown in Figs. S3–S5. The particle sizes of the sulphurized specimens were found to gradually increase as the temperature was raised (Fig. S3). However, the XRD patterns acquired from specimens sulphurized at 600 and 800 °C contained low intensity peaks related to various impurities (Fig. S4). Only the material sulphurized at 700 °C consisted of essentially a single, pure CTGS phase and this same specimen provided a high degree of PEC performance (Fig. S5). Therefore, we concluded that sulphurization at 700 °C was optimal in the present case.

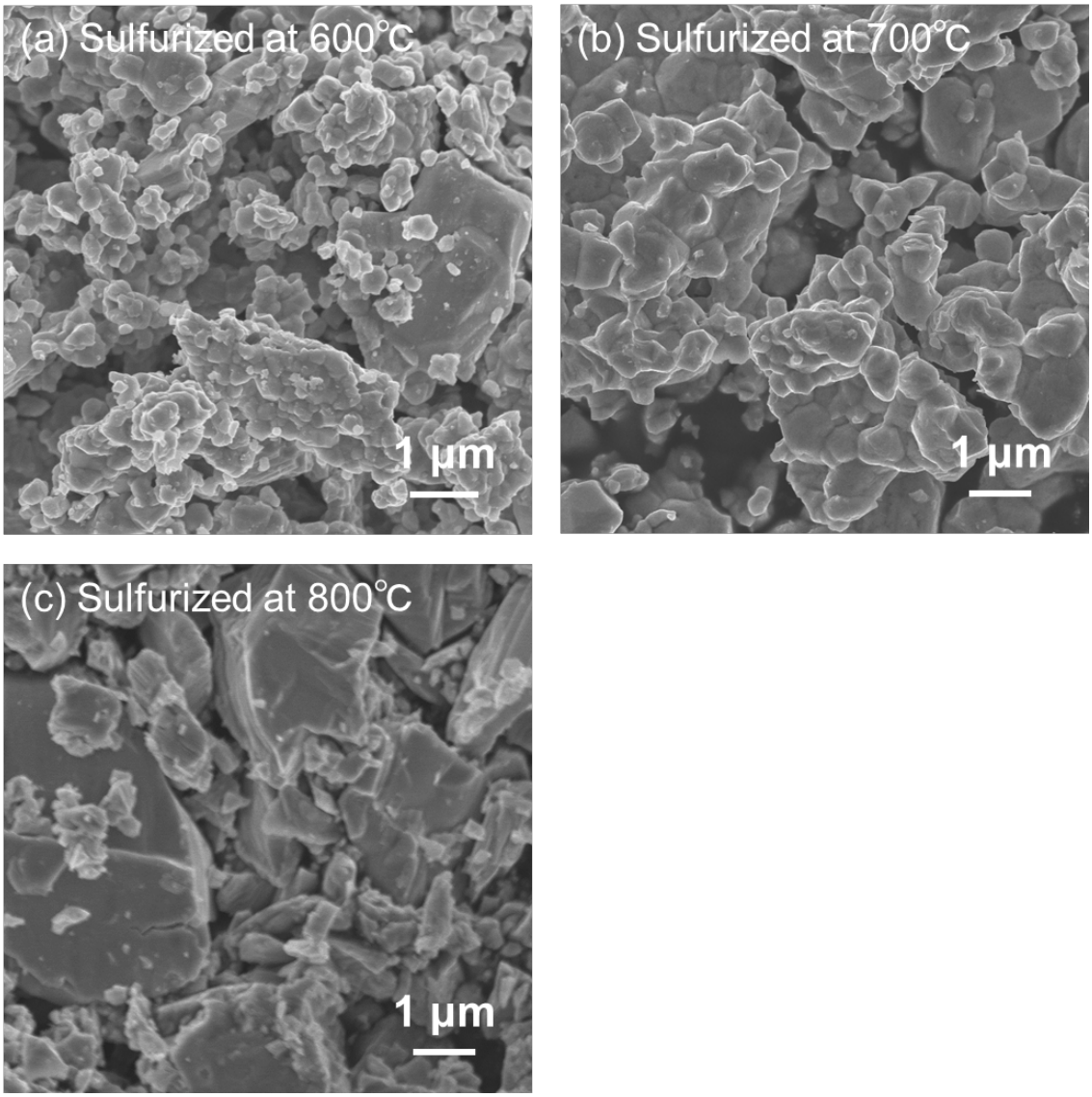


**Fig. S3** SEM images of $Cu_2Sn_{0.5}Ge_{0.5}S_3$ particles synthesized *via* the PC method and subsequent sulphurization at (a) 600, (b) 700, or (c) 800 °C.

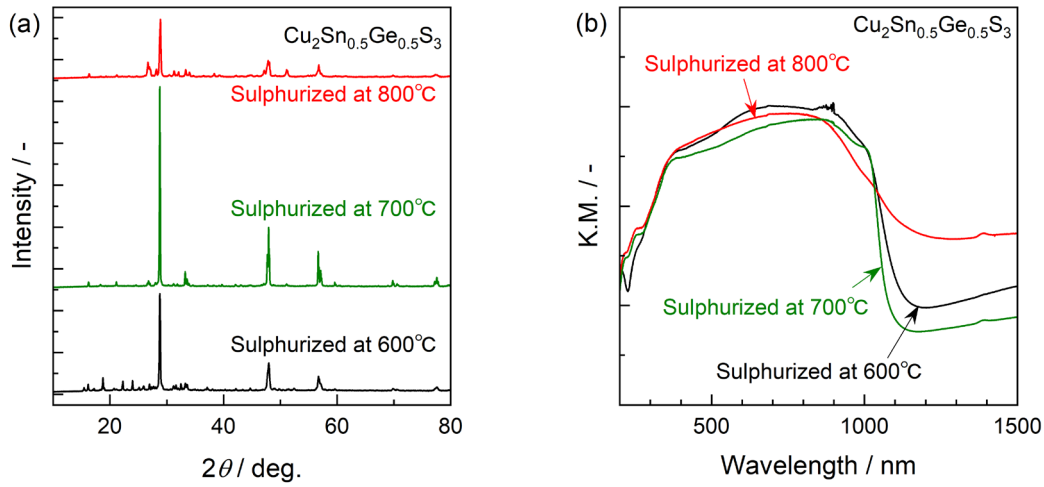


**Fig. S4** (a) XRD patterns and (b) DR spectra of $Cu_2Sn_{0.5}Ge_{0.5}S_3$ particles synthesized *via* the PC method and subsequent sulphurization at various temperatures.

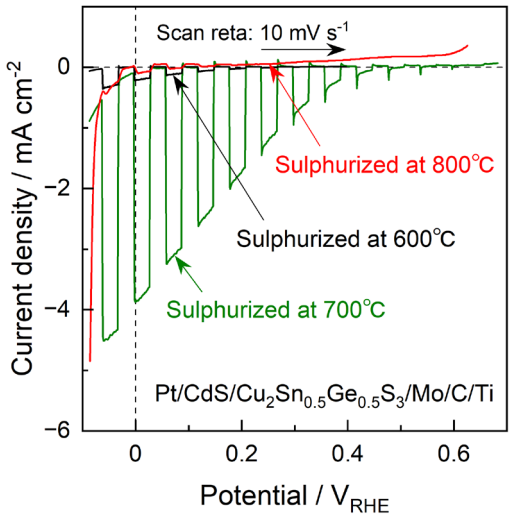


**Fig. S5** Current-potential curves obtained from photocathodes consisting of $Cu_2Sn_{0.5}Ge_{0.5}S_3$ particles synthesized *via* the PC method and subsequent sulphurization at various temperatures. Electrolyte: 1 M KPi (0.5 M $K_2HPO_4$/0.5 M $KH_2PO_4$, adjusted to pH = 7 by KOH). Light source: simulated sunlight (AM 1.5G).

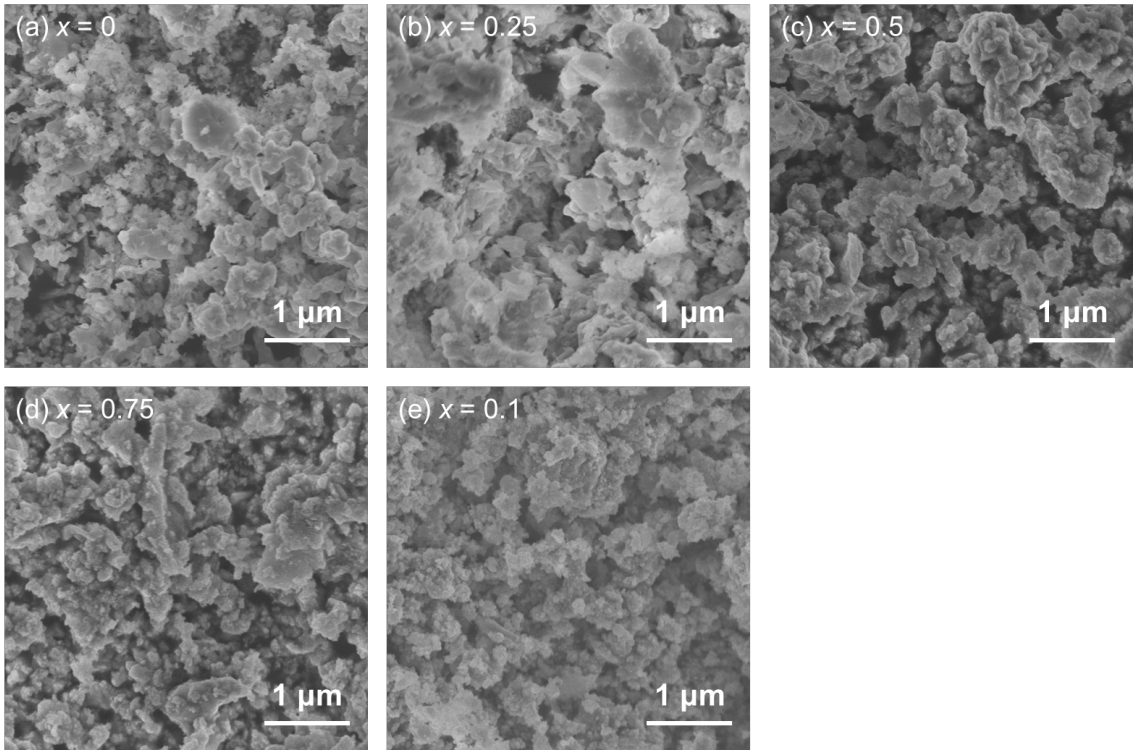


**Fig. S6** SEM images of oxide precursors prepared by the PC method with Sn/(Sn+Ge) values of (a) 0, (b) 0.25, (c) 0.5, (d) 0.75, or (e) 1.

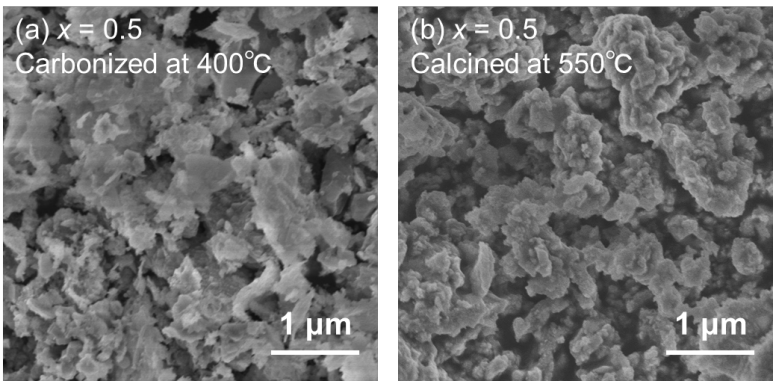


**Fig. S7** SEM images of oxide particles ($x$ = 0.5) prepared using the PC method then (a) carbonized at 400 °C in a mantle heater and (b) subsequently calcined at 550 °C in a muffle furnace.

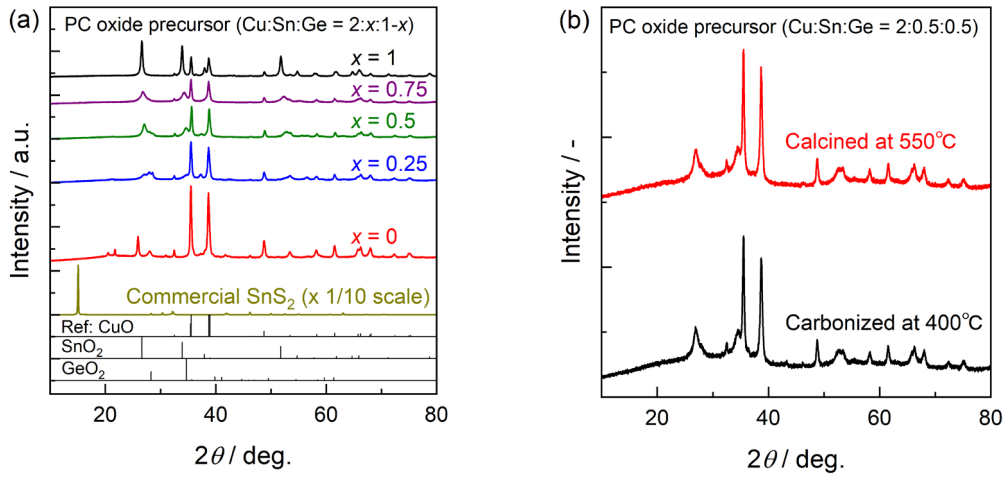


**Fig. S8** XRD patterns for (a) oxide precursors with various Sn/(Sn+Ge) ratios prepared by the PC method together with patterns for a commercial $SnS_2$ reagent (as a representative precursor used in a previous study[2]) on a 1/10 scale and of (b) an oxide precursor prepared by the PC method ($x$ = 0.5) and carbonized at 400 °C in a mantle heater then subsequently calcined at 550 °C in a muffle furnace.

The depth profile of the anion composition involved in the CTGS photocathode was estimated using XPS, with the results presented in Fig. S9. The immediate vicinity of the photocatalyst surface certainly contained O species, whereas slightly smaller S composition than the stoichiometry. Meanwhile, the bulk of CTGS particles comprised little O anions but almost stoichiometric S anions (that is, S/(Sn+Ge) = 3). Thus, it can be concluded that the immediate vicinity of the CTGS surface contained oxidized species, while the bulk of the photocatalytic particles represented pure sulphide.

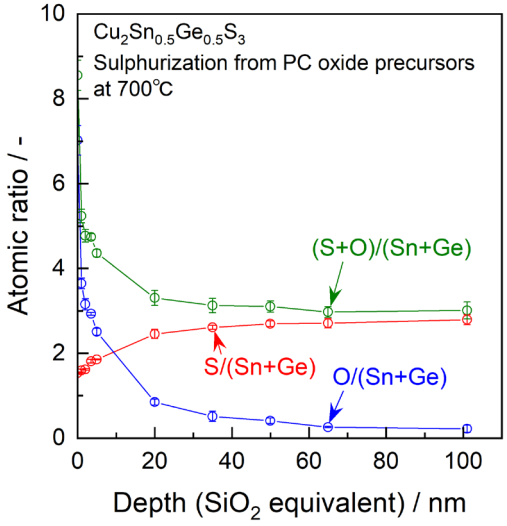


**Fig. S9** Depth profiles of O/(Sn+Ge), S/(Sn+Ge), and (S+O)/(Sn+Ge) determined by XPS.

The particle size distributions of the specimens were found to gradually broaden as the Sn proportion was increased but the distribution of $Cu_2SnS_3$ (that is, the specimens not containing Ge) sharpened (Fig. S10). These effects match the trends observed in the average particle sizes with variations in the Sn/Ge ratio as discussed in the main manuscript. The present specimens prepared by the PC method followed by sulphurization showed unimodal size distributions. Extremely large particles over 10 μm were rarely observed regardless of the Sn/Ge ratio, in contrast to the results obtained using the SSR process.[2]

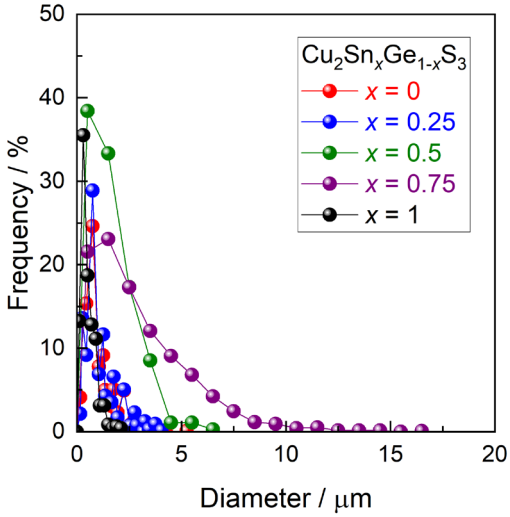


**Fig. S10** Particle size distributions for CTGS particles synthesized *via* the PC method and subsequent sulphurization with various Sn/(Sn+Ge) ratios.

We tried to synthesize the sulphide material by heating the mixture of commercial sulphide precursors under the continuous $N_2$ flow, with the characterization results summarized in Figs. S11 and S12. It was obvious that the SSR method under $N_2$ flow was completely incapable of synthesizing pure phase of CTGS under the present condition (Fig. S11). The specimen showed the undefined shape with wide size distribution (Fig. S12a). Elemental analysis revealed that Ge and S compositions contained in the specimen prepared by the SSR under $N_2$ flow were significantly lower than the stoichiometry (Fig. S12b). The volatile element such as S might be lost during the high temperature treatment under continuous inert gas flow condition, while high temperature should be necessary to obtain highly crystalline photocatalysts. Thus, it can be considered that $H_2S$ flow should be necessary to obtain pure CTGS at the present stage.

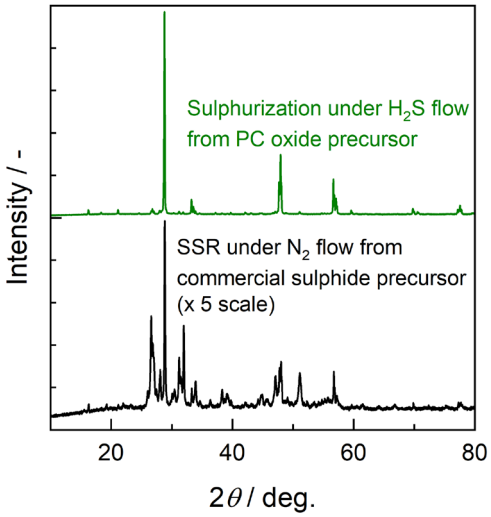


**Fig. S11** XRD pattern obtained from the particulate specimen prepared by heating the mixture of commercial sulphide precursors with Sn/(Sn+Ge) ratio of 0.5 at 700 °C under the continuous $N_2$ flow. XRD pattern of $Cu_2Sn_{0.5}Ge_{0.5}S_3$ particles synthesized through the PC method and subsequent sulphurization is also compiled.

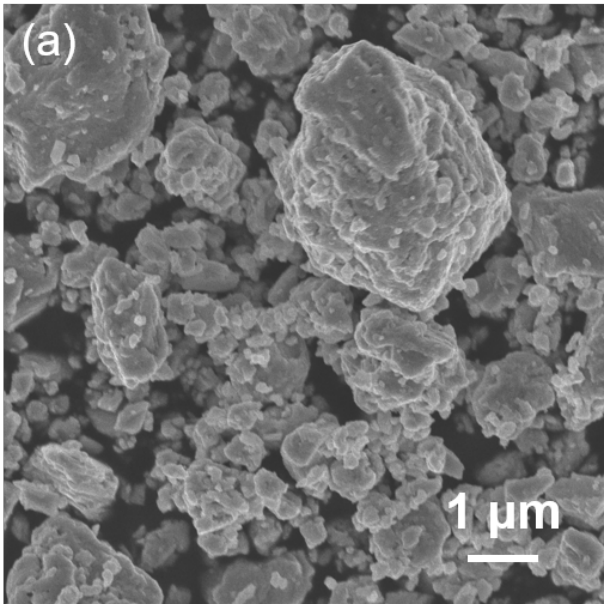


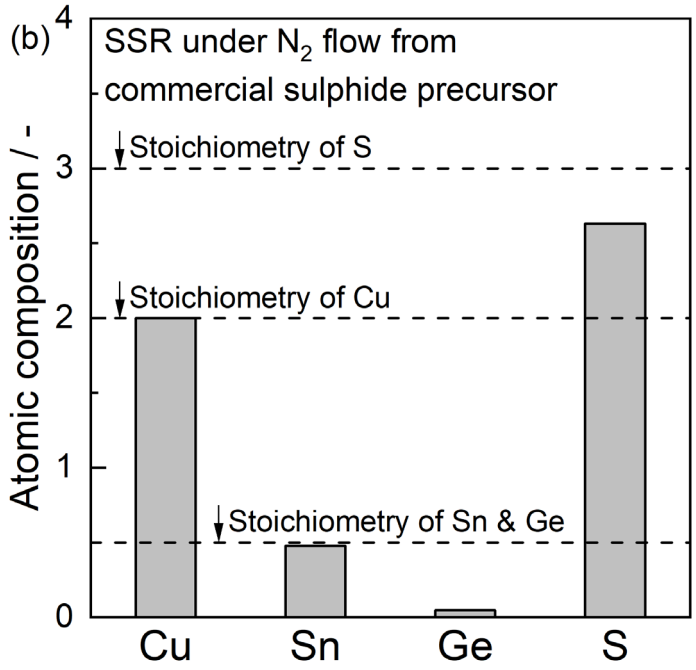


**Fig. S12** (a) SEM image and (b) atomic composition determined by EDS obtained from the particulate specimen prepared by heating the mixture of commercial sulphide precursors with Sn/(Sn+Ge) ratio of 0.5 at 700 °C under the continuous $N_2$ flow. Atomic composition was calculated assuming that the amounts of Cu remained stoichiometry.

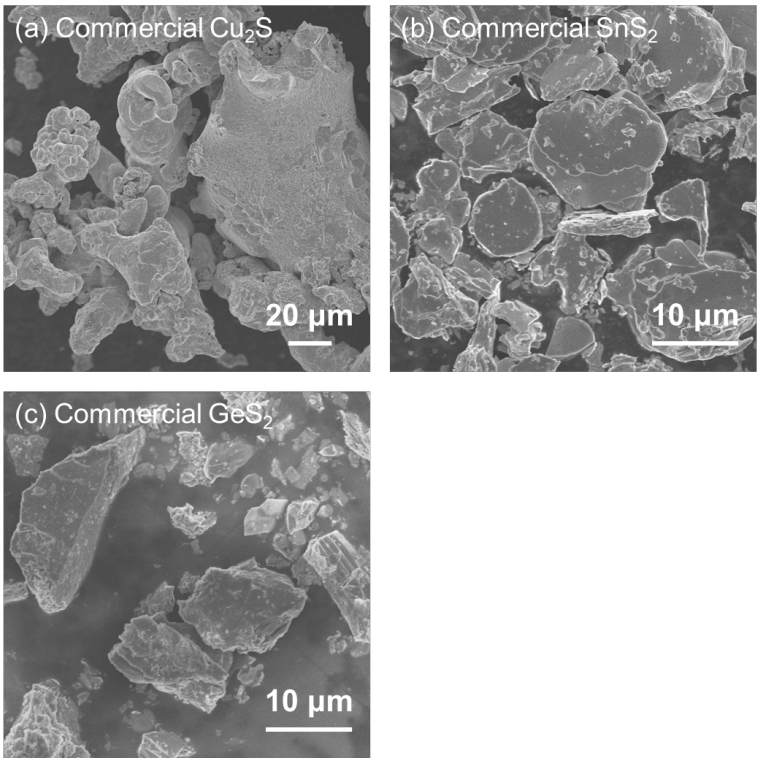


**Fig. S13** SEM images of commercial (a) $Cu_2S$, (b) $SnS_2$, and (c) $GeS_2$ reagents.

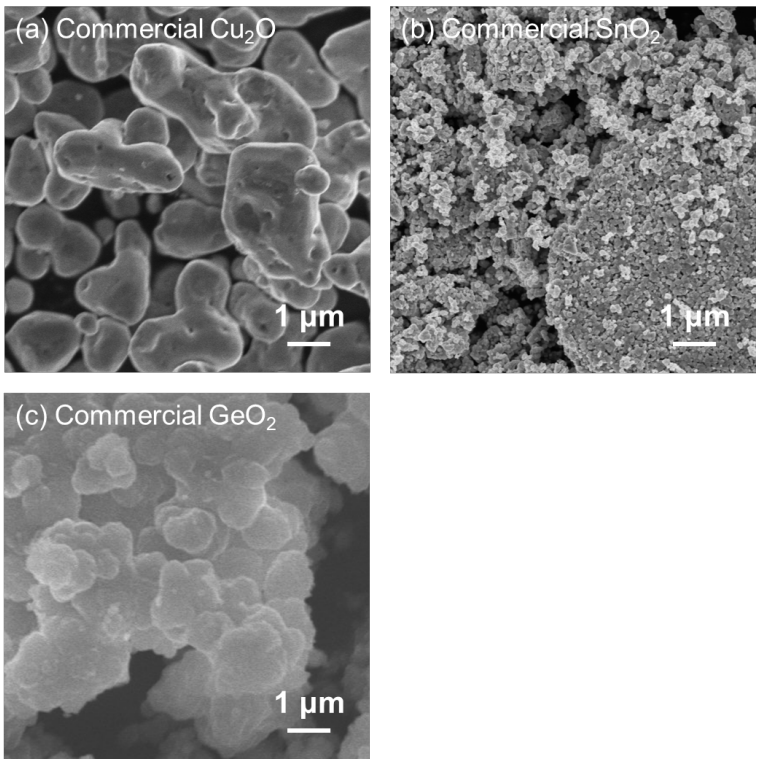


**Fig. S14** SEM images of commercial (a) $Cu_2O$, (b) $SnO_2$, and (c) $GeO_2$ reagents.

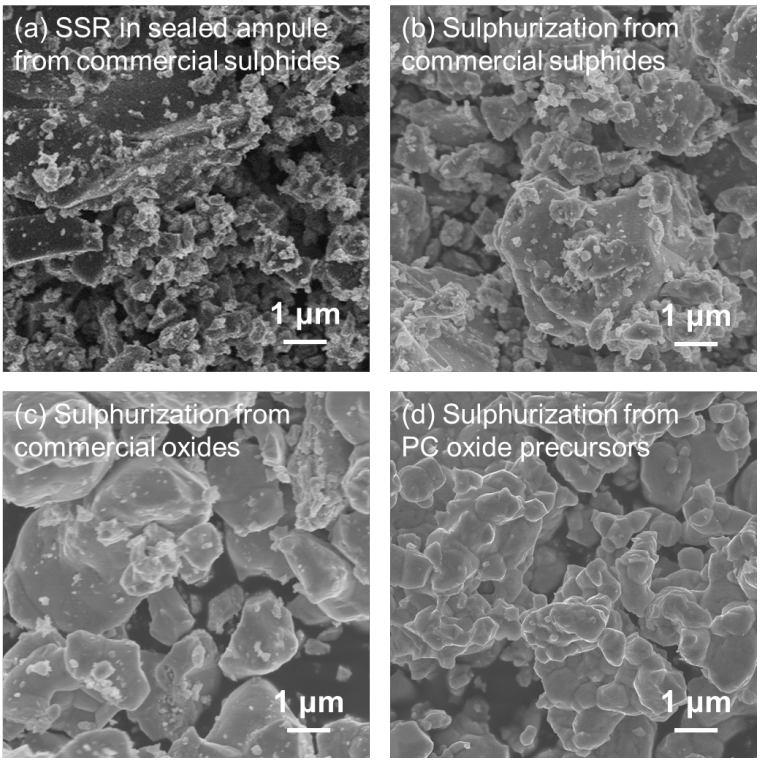


**Fig. S15** SEM images of $Cu_2Sn_{0.5}Ge_{0.5}S_3$ particles synthesized (a) from commercial sulphide precursors using an SSR process in sealed quartz ampules (route 1; conventional method[2]), (b) from commercial sulphide precursors by sulphurization in a tubular furnace under a flow of $H_2S$ (route 2), (c) from commercial oxide precursors by sulphurization (route 3), and (d) from oxide precursors prepared by the PC method followed by sulphurization (route 4; present method).

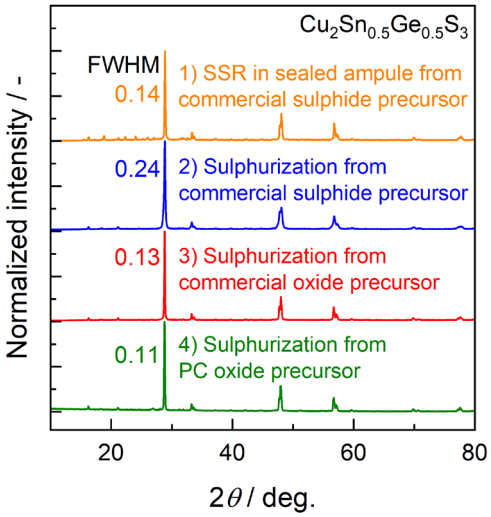


**Fig. S16** XRD patterns acquired from $Cu_2Sn_{0.5}Ge_{0.5}S_3$ particles synthesized from commercial sulphide precursors using the SSR method in sealed quartz ampules (route 1; conventional method[2]), from commercial sulphide precursors by sulphurization in a tubular furnace under a flow of $H_2S$ (route 2), from commercial oxide precursors by sulphurization (route 3), and from oxide precursors prepared by the PC method followed by sulphurization (route 4; present method).

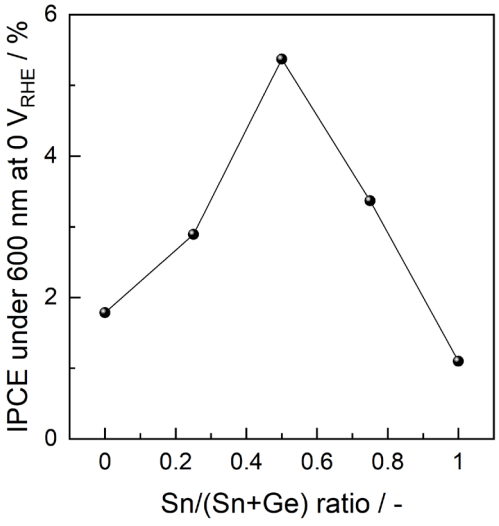


**Fig. S17** IPCEs of CTGS photocathodes having various Sn/Ge ratio obtained under illumination of 600 nm monochromatic light at 0 $V_{RHE}$ of an applied potential as a function of Sn/(Sn+Ge) ratio. It should be noted that the PT photocathodes applied to this experiment were fabricated without substrate heating during the sputtering process of the backside metal electrodes.

We conducted photocatalytic hydrogen evolution experiments using powder suspension system of CTGS synthesized through the conventional SSR and combination of PC method and sulphurization as summarized in Fig. S18. All specimens certainly evolved hydrogen in response to light irradiation. However, CTGS particles prepared by the present method (i.e., sulphurization of PC oxide at 700 °C, which is optimal condition for PEC application) showed lower photocatalytic activity than the specimen prepared by heating the commercial sulphide precursors at 600 °C in a sealed ampule, which is the optimal SSR condition for the photocatalysis application in the previous study.[2] Even when the sulphurization of the PC oxide was performed at 600 °C, the photocatalytic hydrogen evolution rate was barely improved. It can be considered that the present method consisting of PC process and sulphurization might not be suitable to enhance the photocatalytic activity in the powder suspension system. To enhance the photocatalytic activity in the powder suspension, further designing of photocatalyst surface including surface etching and/or loading more appropriate cocatalysts would be necessary.

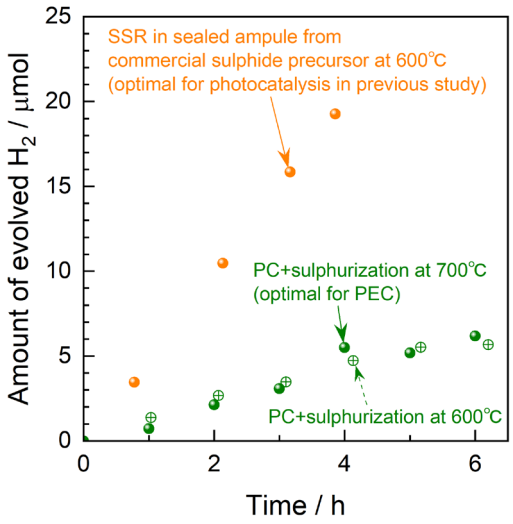


**Fig. S18** Time courses of photocatalytic hydrogen evolution from an aqueous solution containing 10 mM $Na_2S$ and 10 mM $Na_2SO_3$ by using 0.1 g of 1 wt% Ru-modified CTGS particles under full arc irradiation of 300 W Xe lamp.

The onset of X-ray absorption gradually shifted to higher energies in the order of Cu metal, $Cu_2O$ and CuO, reflecting the increased valence state of the Cu in these materials (Fig. S19). The $Cu_2S$ exhibited a similar X-ray absorption onset to that of Cu metal together with a gradual increase in absorption rather than a prominent white line. These results might reflect the electrical conductivity of $Cu_2S$.[3] The present CTGS specimens showed similar X-ray absorption onset characteristics to that of $Cu_2O$, indicating that the Cu incorporated in the CTGS was in the monovalent state. The EXAFS oscillations were also barely affected by the Sn/Ge ratio and the corresponding Fourier transformed radial distribution functions for all specimens each showed a single peak at the same radial distance. These data are consistent with the first nearest-neighbor Cu-S distance values reported in the literature.[4-7]

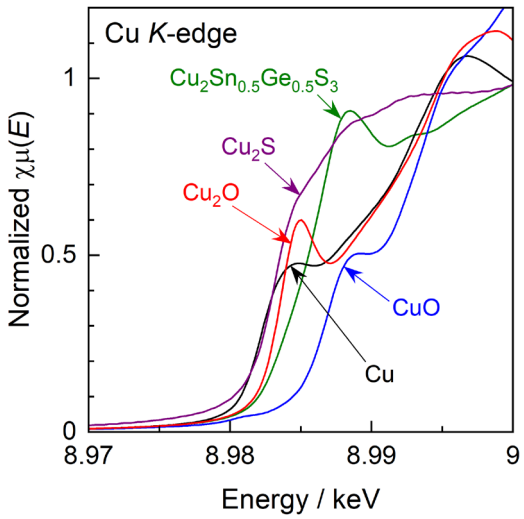


**Fig. S19** Cu *K*-edge XANES spectra of Cu, $Cu_2O$, CuO, $Cu_2S$ and $Cu_2Sn_{0.5}Ge_{0.5}S_3$ synthesized by the sulphurization of an oxide precursor prepared using the PC method.

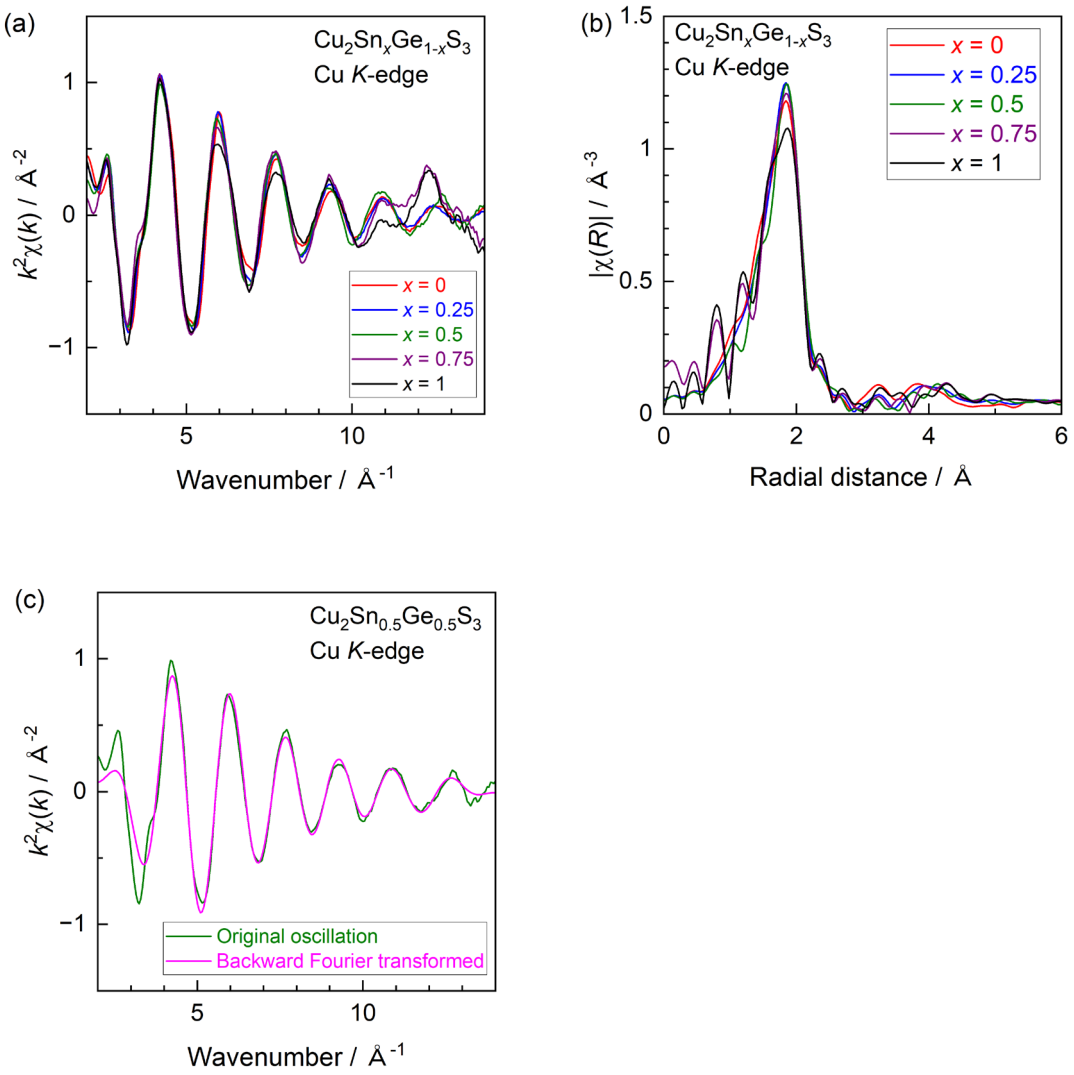


**Fig. S20** (a) Cu *K*-edge $k^2$-weighted EXAFS oscillations and (b) corresponding Fourier transformed radial distribution functions for CTGS particles with various Sn/(Sn+Ge) ratios synthesized by the sulphurization of oxide precursors prepared using the PC method. (c) Comparison of experimental and fitted EXAFS data. The *k*-range applied for the Fourier transformation is 3 – 13 Å$^{-1}$, while the *R*-range applied for the backward Fourier transformation is 1 – 3 Å.

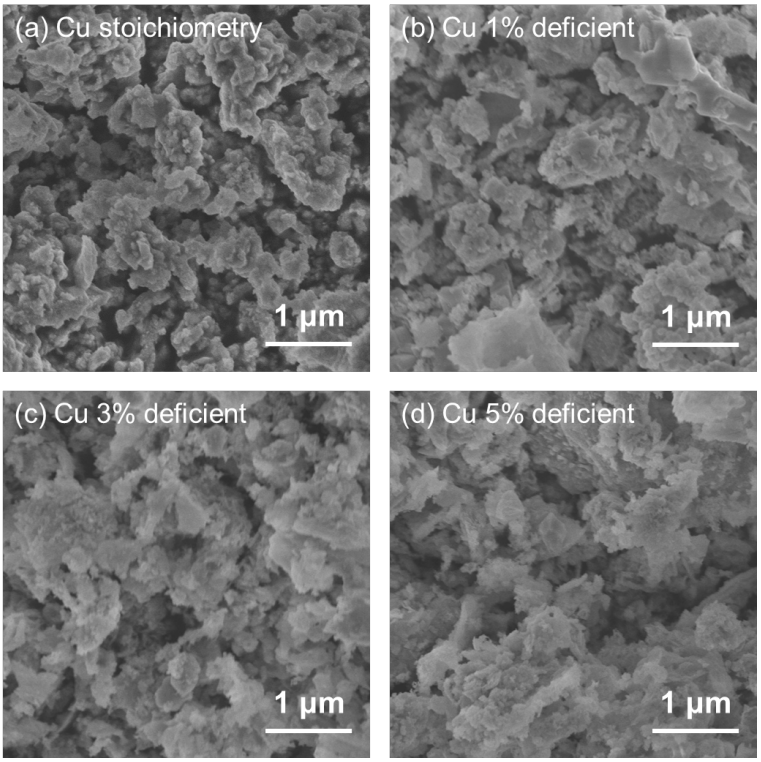


**Fig. S21** SEM images of oxide precursors prepared by the PC method with a Sn/(Sn+Ge) ratio of 0.5 and various Cu proportions: (a) stoichiometric, (b) 1% Cu deficient, (c) 3% Cu deficient, and (d) 5% Cu deficient.

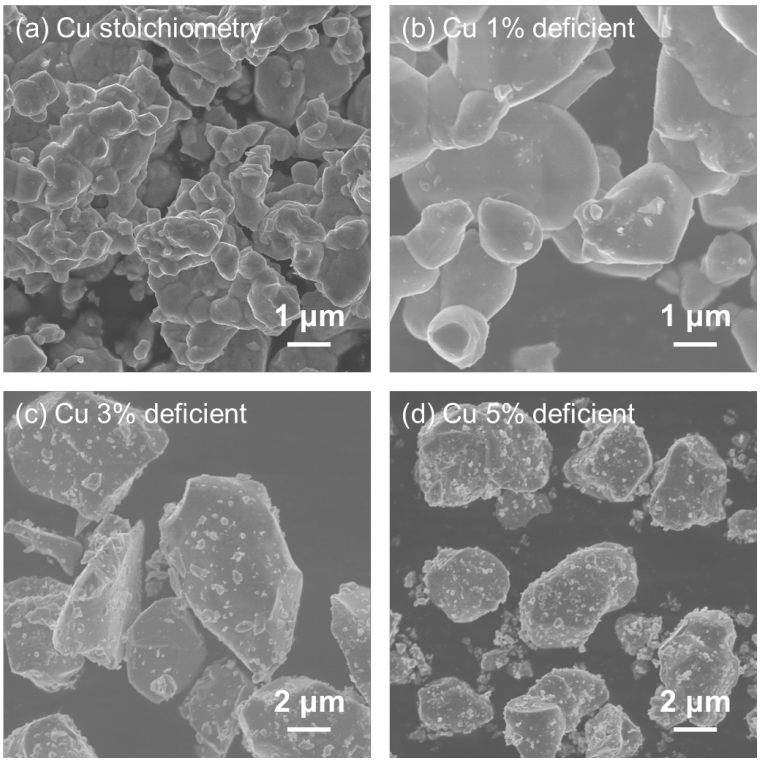


**Fig. S22** SEM images of CTGS particles synthesized by the PC method and subsequent sulphurization with a Sn/(Sn+Ge) ratio of 0.5 and various Cu proportions: (a) stoichiometric, (b) 1% Cu deficient, (c) 3% Cu deficient, and (d) 5% Cu deficient.

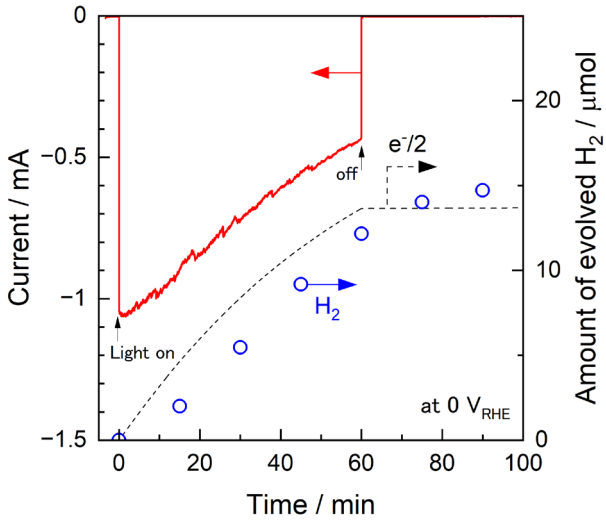


**Fig. S23** Time courses of the cathodic photocurrent, the expected amount of evolved $H_2$ as calculated based on $e^-/2$ values, and the actual amounts of $H_2$ detected by microGC during a PEC reaction using a Pt/CdS/$Cu_{1.94}Sn_{0.5}Ge_{0.5}S_3$ photocathode in 1 M KPi (0.5 M $K_2HPO_4$ / 0.5 M $KH_2PO_4$, adjusted to pH = 7 with KOH) under simulated sunlight (AM 1.5G).

## References


1. H. G. Langer, Solid complexes with tetravalent metal ions and ethylenediamime tetra-acetic acid (EDTA), *J. Inorg. Nucl. Chem.*, 1964, **26**, 59–72.
2. Y. Kageshima, S. Shiga, T. Ode, F. Takagi, H. Shiiba, M. T. Htay, Y. Hashimoto, K. Teshima, K. Domen and H. Nishikiori, Photocatalytic and Photoelectrochemical Hydrogen Evolution from Water over $Cu_2Sn_xGe_{1-x}S_3$ Particles, *J. Am. Chem. Soc.*, 2021, **143**, 5698–5708.
3. P. Kumar, R. Nagarajan and R. Sarangi, Quantitative X-ray absorption and emission spectroscopies: electronic structure elucidation of $Cu_2S$ and CuS, *J. Mater. Chem. C*, 2013, **1**, 2448–2454.
4. R. Bacewicz, J. Antonowicz, S. Podsiadło and S. Schor, Local structure in $Cu_2ZnSnS_4$ studied by the XAFS method, *Solid State Commun.*, 2014, **177**, 54–56.
5. P. T. Erslev, M. R. Young, J. V. Li, S. C. Siah, R. Chakraborty, H. Du, R. J. Lad, T. Buonassisi and G. Teeter, Tetrahedrally coordinated disordered $Cu_2SnS_3$–$Cu_2ZnSnS_4$–ZnS alloys with tunable optical and electronic properties, *Sol. Energy Mater. Sol. Cells*, 2014, **129**, 124–131.
6. W. Hu, J. Ludwig, B. Pattengale, S. Yang, C. Liu, X. Zuo, X. Zhang and J. Huang, Unravelling the Correlation of Electronic Structure and Carrier Dynamics in $CuInS_2$ Nanoparticles, *J. Phys. Chem. C*, 2018, **122**, 974–980.
7. M. J. Turnbull, Y. M. Yiu, M. Goldman, T.-K. Sham and Z. Ding, Favorable Bonding and Band Structures of $Cu_2ZnSnS_4$ and CdS Films and Their Photovoltaic Interfaces, *ACS Appl. Mater. Interfaces*, 2022, **14**, 32683–32695.